RESEARCH ARTICLE

Research on Dynamic Seal Friction Torque Compensation for a Low-Slow-Small UAV Tracking System

ZHUQIU GAI AND JINSONG WANG

School of Optoelectronic Engineering, Changchun University of Science and Technology, Changchun 130022, China

Corresponding author: Jinsong Wang (Soldier_1973@163.com)

ABSTRACT To ensure reliable and accurate operation in a complex field environment for Low-Slow-Small unmanned aerial vehicle (LSS-UAV) tracking systems, a dynamic seal shafting structure consisting of a labyrinthine structure and a magnetic fluid seal ring is designed to protect important equipment, such as the infrared sensor, visible CCD and the laser rangefinder from erosion and oxidation by the external environment. A friction torque model is established for the system's dynamic seal structure to ensure tracking accuracy of the system. The simulation results show that the closed-loop speed accuracy of the system is improved by nearly 10 fold after adding friction torque compensation. The actual test results show that including friction torque compensation can effectively reduce the start-up delay and speed fluctuation error, and the speed fluctuation error is reduced by more than 80% compared to that without friction torque compensation. The tracking accuracy of the dynamic LSS-UAV is reduced from 56.44 μrad to 14.86 μrad after adding friction torque compensation, which meets the requirement of smooth and accurate tracking for LSS-UAV tracking systems, and verifies the effectiveness and accuracy of compensation for the dynamic seal friction torque.

INDEX TERMS Friction torque, LuGre, magnetofluid, tracking system.

I. INTRODUCTION

Unmanned aerial vehicles (UAVs) are widely used in the fields of video shooting, news reporting, geographic mapping, search and rescue and military reconnaissance, for example, which has greatly improved work efficiency in these areas. However, the existence of illegal flights poses a potential security risk to the flight safety of the airport, the security of major event sites and important military facilities, and some lawbreakers even use UAVs to engage in unlawful investigation, drug trafficking, smuggling and other unauthorized and criminal activities [1], [2], [3]. With the application of UAV drone bee colony technology, the three-dimensional attack mode formed by various small unmanned equipment poses a new challenge to the defense systems of all

The associate editor coordinating the review of this manuscript and approving it for publication was Atif Iqbal.

countries [4], [5], [6].Therefore, there is an urgent need to research detection equipment for small UAVs flying at low altitudes and with slow flying speed (LSS-UAVs). At present, there are three commonly used locating methods: radar detection, acoustic detection and photoelectric detection, of which the photoelectric detection method can use the sensitivity of infrared detectors to thermal targets and easy to find small targets; and the infrared image can intuitively reflect the characteristics of the target, allowing distinguishing from similar targets such as flocks of birds, thereby improving the success rate of system detection [7].

After the photoelectric tracking system finds and locks an LSS-UAV, the UAV can be driven away by jamming devices or destroyed by a laser. The photoelectric tracking system needs to have a very high follow-up tracking performance to ensure the damage effect. Photoelectric tracking systems mostly work in the wilderness, deserts, mountains and other

harsh environments. To protect important sensors of the tracking system such as the CCD camera, infrared camera, laser range finder or signal jamming equipment, dynamic sealing technology is often used to solve problems of rain, dust or oxidation. In the past, many methods including filling felt oil rings or extruding U-shaped sealing rings in labyrinth structures were used [8], [9], [10], but both these examples cannot achieve a complete state of airtightness and water tightness. Moreover, they bring great friction interference torque to the servo control system, seriously affecting the low-speed stability and speed control accuracy of the detection system [11], which further affects the tracking accuracy of the target, and reduces the damage effect of the system's jammer or laser on the target.

Magnetofluid sealing technology is a magnetic fluid sealing ring formed using a magnetic fluid under the action of a magnetic field, through which it can form a closed space of direct contact between the motion shaft system. This can effectively seal the gas and liquid and avoiding direct friction between the moving shaft system and the sealed construction. The typical design and working principle of a centrifugal magnetic fluid shaft seal were presented in [12]. Application of magnetofluid sealing technology to the dynamic sealing structure of aerospace engineering cylinders was introduced in [13]. The technology was applied to the shaft sealing structure of a rotary blood pump, and a satisfactory sealing effect was achieved [14]. We apply this magnetofluid sealing technology to an LSS-UAV photoelectric tracking system. The structural diagram of the pitch shafting of the photoelectric tracking system is shown in Fig.1. In the shafting structure, the U-shaped pitch frame is connected to the sealing load cabin that contains important sensors, such as the infrared sensor, visible CCD and the laser rangefinder via a magnetofluid sealing ring that prevents the sensors from being eroded by rain, dust or air oxidation. To ensure the system's reliability, a labyrinth structure and sealed hatch cover are designed as auxiliary sealing structures.
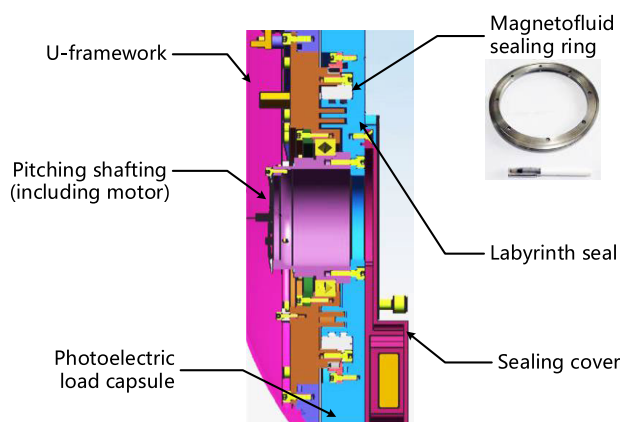

FIGURE 1. Seal structure diagram.

To measure the friction torque of the rotating shaft system accurately and compensate for it, many scientists, researchers

and engineers have carried out related research [15]. Cho, Seong-Hee et al. used a torque sensor to directly measure the friction torque caused by harmonic gears, and fitted friction models with a quantic polynomial [16]; Kim, MJ et al. observed friction torque by using the method of a frictionless model observer, and verified using in an example of a 7-link surgical robot [17]. PL Cui applied a time delay estimator to estimate the nonlinear friction torque of a system and compensated for it by combining with a two-degree-of-freedom internal model control, realizing high precision control of a gimbal servo system. The compensation measures based on the LuGre friction torque model were adopted in [21], [22], [23], [14], [25], and [26], and satisfactory compensation results were obtained.

We take the respective friction torque caused by the magnetic fluid sealing ring, labyrinth structure and rotating shaft system as the comprehensive friction torque, and measure the real-time data of this overall friction torque as it changes with the driving current. An appropriate frictional moment model is then used for fitting. Using the fitting analysis of the experimental data, we found that curve fitting adopting the LuGre friction model could accurately describe the comprehensive friction torque of the system. Simulation and experimental analyses showed that after complete friction compensation, the low-speed start-up delay and speed fluctuation error of the photoelectric tracking system was effectively reduced, and the tracking accuracy of LSS-UAV efficiently improved.

II. FRICTION TORQUE IDENTIFICATION

Besides the accuracy of speed feedback sensors (such as gyroscopes or shaft angle encoders), the speed control accuracy of a tracking system is influenced mainly by external disturbances (such as wind resistance, temperature, etc.) as well as the comprehensive friction torque disturbance of its shafting. The external disturbances can be compensated for by designing a disturbance observer that observes the disturbance torque. The comprehensive friction torque of the shafting needs to be measured or observed by observers and compensated for in real-time. From previous studies, many friction torque models have been proposed, such as the Dahl model, Bristle model, LuGre model, Leuven model and Maxwell-slip model, for example. Among them, the LuGre model can describe well the dynamic and static friction characteristics of friction, such as pre-sliding displacement, crawling, friction memory, variable static friction and the Stribeck curve.

A. MODEL OF FRICTION TORQUE
The LuGre model describes the functional relationship between the friction torque and relative velocity and the displacement in the pre-sliding and sliding stages, which can reflect both the static and dynamic characteristics of friction. The friction torque is given by

$$T_f = \sigma_0 z + \sigma_1 \frac{dz}{dt} + \sigma_2 \dot{\theta}, \qquad (1)$$

where, T_f is the friction torque, z is the average bristle deformation of the shafting contact surface, θ is the relative rotational speed of the shafting, σ_0, σ_1 and σ_2 are called the stiffness coefficient of bristles in the pre-sliding stage, damping coefficient of the bristles and viscous coefficient of the friction respectively. The derivative of the average deformation of the bristle concerning time is given by

$$\frac{dz}{dt} = \dot{\theta} - \frac{\sigma_0 \left| \dot{\theta} \right|}{g\left(\dot{\theta}\right)} z. \tag{2}$$

Equation (3) represents the Stribeck effect:

$$g\left(\dot{\theta}\right) = T_c + (T_s - T_c) e^{-\left(\frac{\dot{\theta}}{\dot{\theta}_s}\right)^2}, \tag{3}$$

where, T is the maximum static friction torque, T is the Coulomb friction torque and $\dot{\theta}_s$ is the switching speed for the Stribeck effect.

The purpose of friction modeling is to apply a friction model that compensates, controls and minimizes the adverse effects of friction. Identification of friction parameters in a system is the basis to achieve this goal. The friction torque model described by the LuGre model can be divided into two stages: the pre-sliding and sliding stages. So, we can split the corresponding friction parameter identification into dynamic parameter identification and static parameter identification. As the friction torque is related to the direction and speed of the rotational speed of the equipment, we define the clockwise rotation of the equipment as the positive speed direction and take the direction as an example for identifying the dynamic and static parameters of the friction torque model. The principle and method of the negative direction parameter identification are similar.

B. STATIC PARAMETER IDENTIFICATION FOR LUGRE MODEL

When the system is in a stable sliding state, we can infer that $dz/dt=0$. According to this condition, we may rewrite equation (2) as

$$\sigma_0 z = \frac{\dot{\theta}}{\left| \dot{\theta} \right|} g(\dot{\theta}) = g(\dot{\theta}) \cdot sgn(\dot{\theta}). \tag{4}$$

Substituting (4) into (1) leads to

$$T_f = [T_c + (T_s - T_c) e^{-\left(\frac{\dot{\theta}}{\dot{\theta}_s}\right)^2}] \cdot sgn(\dot{\theta}) + \sigma_2 \dot{\theta}. \tag{5}$$

It is necessary to identify the four parameters T_s, T_c, θ_s and σ_2 before calculating T_f.

Supposing that the total rotary inertia of the system is J, the axial angular acceleration is $\ddot{\theta}$, the input of the control torque is u, the friction torque of the system is T_f, and the disturbance torque caused by wind resistance, mass imbalance, and wire disturbance is T_d, the dynamics equation of the system is given by

$$J\ddot{\theta} = u - (T_f + T_d). \tag{6}$$

We can deduce that $u - (T_f + T_d) = 0$ if the equipment runs at a constant speed. Without considering the influence of T_d for the time being, we can conclude that

$$u = T_f. \tag{7}$$

According to (7), the equipment can run stably at different speeds, and the corresponding control current can be measured at the same time, and then the measured data can be fitted to obtain the static friction torque model that varies with the speed. Figure 2 shows the friction torque fitting curve of the system according to the positive speed direction obtained by an experiment in which the abscissa is the rotational speed of the system, and the ordinate is the current code value collected by the analog-to-digital converter. The Stribeck curve is fitted according to (5), and the values of the four parameters identified are shown in Table 1.
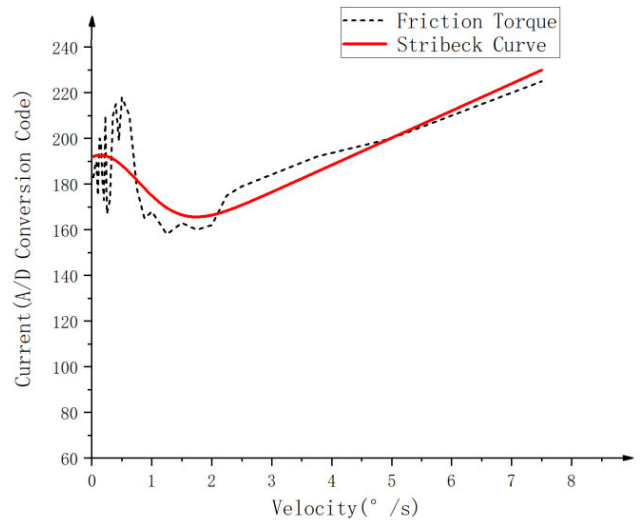

FIGURE 2. The fitting curve of friction torque.

TABLE 1. Static parameter identification.

T_s	T_c	θ_s	σ_2
191.79	140.84	1.09	11.88

C. DYNAMIC PARAMETER IDENTIFICATION OF LUGRE MODEL

Pre-sliding state refers to the state when the system is static macroscopically, but there is still a slight displacement change microscopically. In this state, the speed is in critical motion or very low-speed motion. Thus, it can be approximately assumed that

$$|z| \ll g\left(\dot{\theta}\right). \tag{8}$$

Applying (8) to (2), we obtain

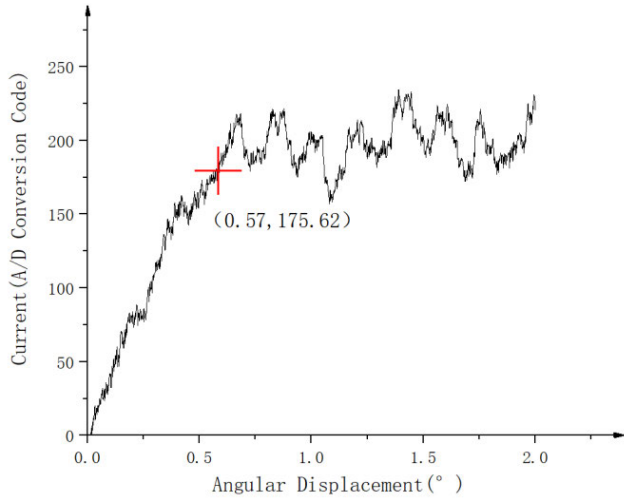$$\frac{dz}{dt} \approx \dot{\theta}, z \approx \theta. \tag{9}$$

FIGURE 3. Relationship curve between the current and angle position.

According to (1), the friction torque in the pre-sliding stage can be described as:

$$T_f = \sigma_0\theta + (\sigma_1 + \sigma_2)\,\dot\theta. \tag{10}$$

Substituting (10) into (6) while ignoring the influence leads to

$$J\ddot\theta + (\sigma_1 + \sigma_2)\,\dot\theta + \sigma_0\theta = u. \tag{11}$$

Laplace transformation is performed on the above equation to obtain:

$$Js^2\theta(s) + (\sigma_1 + \sigma_2)\,s\theta(s) + \sigma_0\theta(s) = U(s). \tag{12}$$

From this, we obtain

$$\varphi(s) = \frac{\theta(s)}{U(s)} = \frac{1}{Js^2 + (\sigma_1 + \sigma_2)\,s + \sigma_0}, \tag{13}$$

which can be approximated as a second-order damping system. Assuming that the damping ratio of the second-order system is ζ and the natural oscillating frequency is ω_n, we can get:

$$\varphi(s) = \frac{1}{Js^2 + (\sigma_1 + \sigma_2)\,s + \sigma_0} = \frac{1}{s^2 + 2\zeta\omega_n s + \omega_n^2}. \tag{14}$$

By comparing the coefficients of the corresponding denominator polynomials, we can deduce that

$$\sigma_1 + \sigma_2 = 2\zeta\sqrt{J\sigma_0}, \tag{15}$$

where σ_0 can be estimated by the slight displacement generated in the pre-sliding stage and the corresponding control value. In the pre-sliding stage, it can be assumed that $\dot\theta \approx 0$, $\ddot\theta \approx 0$, $z \approx 0$. So, according to (11), it can be concluded that

$$\sigma_0 = \frac{u}{\theta}. \tag{16}$$

Inputting a small control value to the system to obtain the relationship curve between control current and angle position as shown in Fig.3.

Hence, we can calculate that

$$\sigma_0 = \frac{\Delta u}{\Delta\theta} = 308.1.$$

Assuming that the optimal damping ratio is $\zeta = 0.707$ and the rotatory inertia of the system is $J = 23.5$, it can be further obtained from (15) that

$$\sigma_1 = (2J\sigma_0)^{1/2} - \sigma_2 = 108.46.$$

So far, we have obtained the identification results of four static parameters including T_s, T_c, θ_s, σ_2 and two dynamic parameters including σ_0 and σ_1 of the LuGre friction torque model.

III. SIMULATION OF COMPENSATION FOR FRICTION TORQUE

Using the identified parameters, the LuGre friction torque model is established using Matlab software, as shown in Fig. 4.
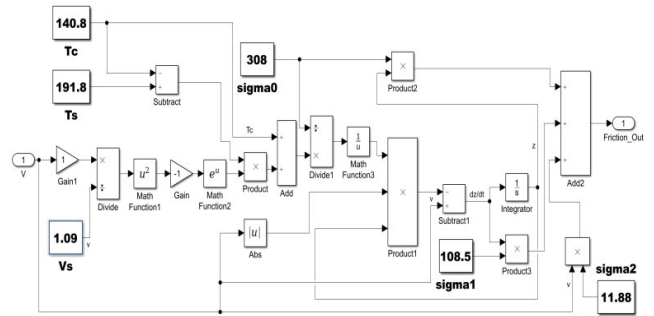

FIGURE 4. Simulation model of LuGre friction torque.

Further, the simulation model of the DC torque motor is established as shown in Figure.5:
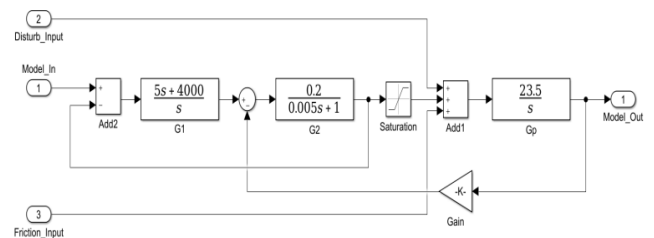

FIGURE 5. Simulation model of the DC motor.

A closed-loop speed simulation system is built based on the created friction torque model and the controlled object model, as shown in Fig. 6.

A traditional PI controller is adopted in the controller, and a sinusoidal signal with an amplitude of 1°/s and a frequency of 0.1Hz is used as the input test signal. After simulation, the closed-loop output simulation curve of speed is obtained as shown in Fig. 7.

From the figure, we can see the influence of friction on the system speed output at low speed and the speed commutation stage. To further simulate the low-speed start-up
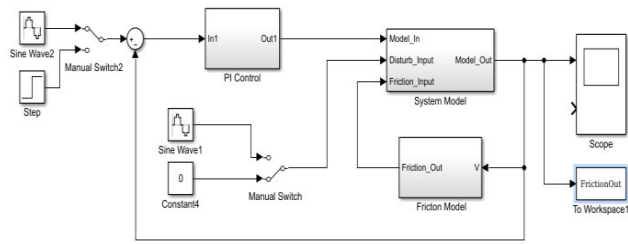
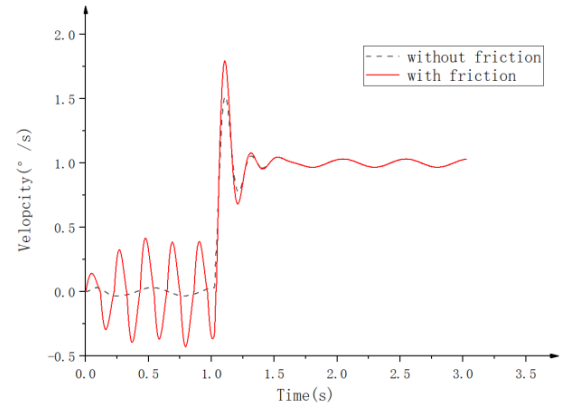**FIGURE 6.** System simulation with LuGre friction torque model.

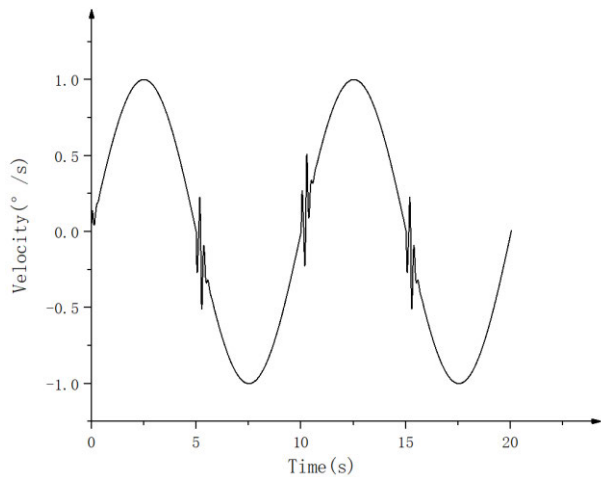**FIGURE 7.** System simulation with LuGre friction torque model.

of the system, a speed step test signal with an amplitude of 1°/s was conducted as a sinusoidal disturbance signal with an amplitude of 0.02°/s, and a frequency of 2 Hz was added to the system, which was the compared with the model without friction torque, as shown in Figure. 8:
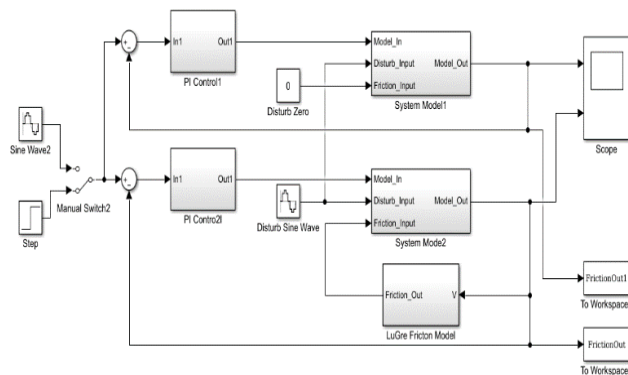

FIGURE 8. Simulation of the system with a friction torque model.

It can be seen from the simulation output curve of Fig. 9 that the system needs to overcome the friction force in the low-speed start-up stage, resulting in a repeated oscillation of the speed. In addition, compared with the friction-free model, the overshoot of the step response of the system increases

FIGURE 9. Influence of friction on the low-speed step response.

by 25%, which has a negative impact on the low-speed stability of the system.

To eliminate the influence of friction torque on the speed control accuracy of the system, a friction torque compensation module is added, as shown in Figure 10. At the same time, to eliminate the influence of the external speed disturbance signal on the speed control accuracy of the system, a disturbance observer is added to the simulation system.
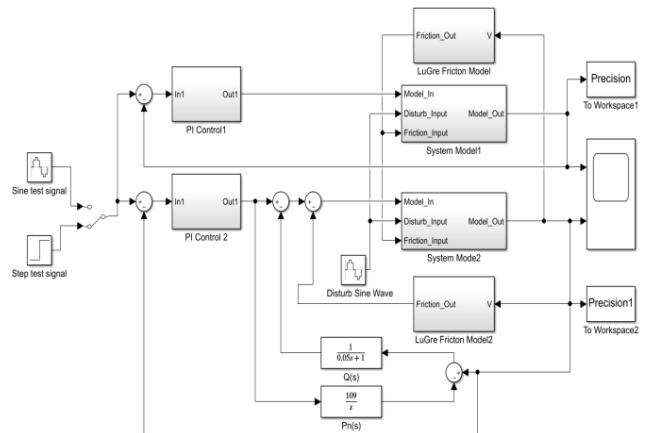

FIGURE 10. Simulation model of compensation of friction torque.

After inputting the same sinusoidal speed test signal with an amplitude of 1°/s and frequency of 0.1 Hz to the simulation system, the response curves are shown in Fig. 11.

Fig. 11 (a) shows the response curve of the system without friction torque compensation. It can be seen that the response curve is seriously affected by friction in the low-speed stage and the speed fluctuation is obvious. Fig. 11 (b) is the response curve of the system after adding the velocity disturbance observer (VOB). It can be seen from the local enlarged area that although the disturbance observer can reduce the impact of friction torque disturbance on the speed output accuracy in the low-speed stage, it still cannot completely overcome the impact of friction force on the speed output accuracy. Fig. 11 (c) shows the speed output curve of the system when disturbance observer and friction torque
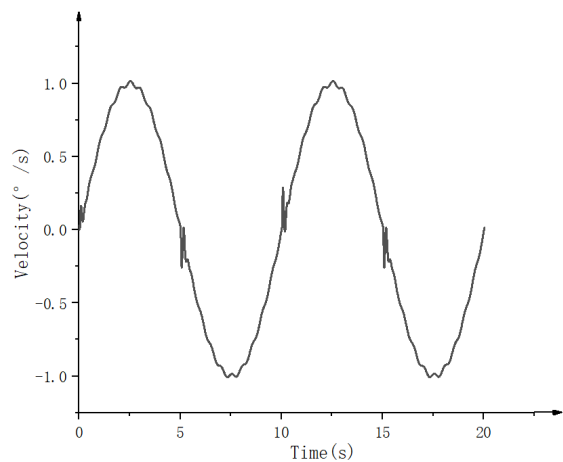
(a) **Without compensation for Friction.**
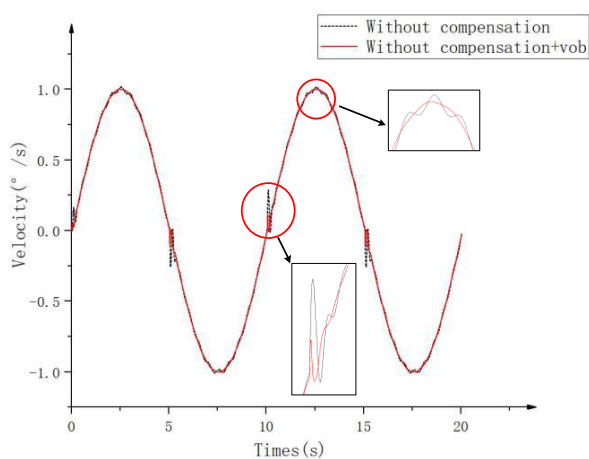
（b）**Adding VOB without friction torque compensation.**
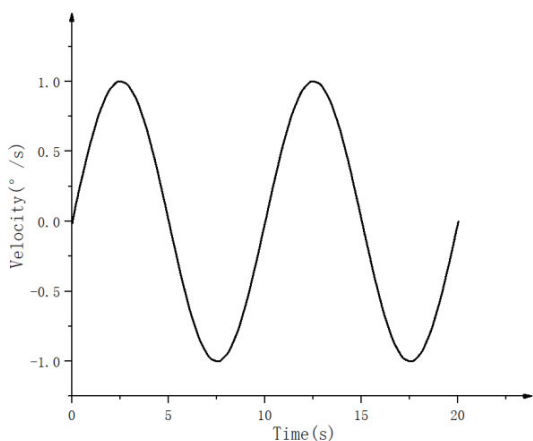
（c）**Adding VOB with friction torque compensation.**

FIGURE 11. Compensation curves with and without Friction torque.

compensation are added to the system at the same time. It can be seen that the friction torque of the system is overcome in the low-speed stage, and the disturbance of the system is also effectively eliminated.

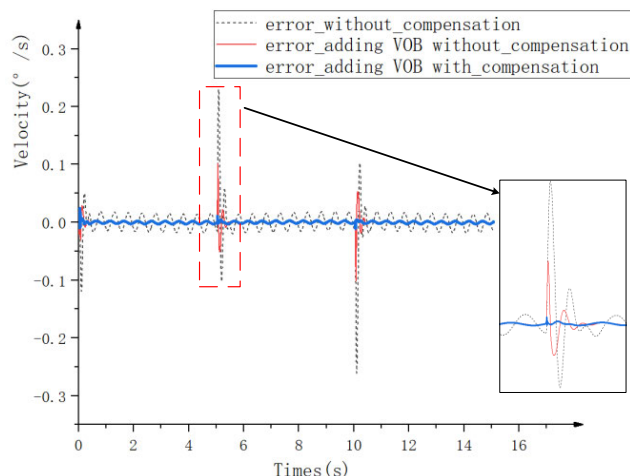The system output error is shown in Figure 12.

FIGURE 12. The speed error curve.

It can be deduced from in Fig.12 that the output error of the system is close to $\pm 0.25°$/s without friction torque compensation, while the output error of the system is about $\pm 0.02°$/s with friction torque and disturbance observer compensation, an increase of about 10 fold.

It can be seen that adding friction torque compensation to the system can effectively restrain the influence of friction on the control accuracy at the low-speed stage of the system. If the velocity disturbance observer is added, the system's low-speed stability and control accuracy can be further improved.

IV. EXPERIMENTS

A. COMPOSITION OF EXPERIMENTAL SYSTEM

The LSS-UAV tracking system consists of a two-degree-of-freedom tracking frame and a sealed load cabin. The tracking frame is mainly composed of dynamic seal shafts, DC torque motors, angle sensors and servo controllers, which can realize closed-loop speed and closed-loop position control for azimuth and pitch degrees. The sealed load cabin is equipped with a visible CCD, infrared sensor, laser rangefinder, gyroscope and other sensors. The load cabin is connected to the tracking frame by the dynamic sealing structures. The inside of the cabin is filled with nitrogen as a protective gas against oxidation. A composite dynamic seal structure is adopted in azimuth axis system. In the experiment, the azimuth shafting is taken as the experimental object, and the ability of the friction torque model to overcome the friction torque in the low-speed movement stage of the system is investigated. The system is shown in Fig.13:

B. EXPERIMENT WITH FRICTION TORQUE COMPENSATION

Because the system is in the start-up stage, without friction torque compensation, the system needs to overcome the influence of friction torque, so the start-up speed of the system will have obvious speed delay, and the stability of the speed will
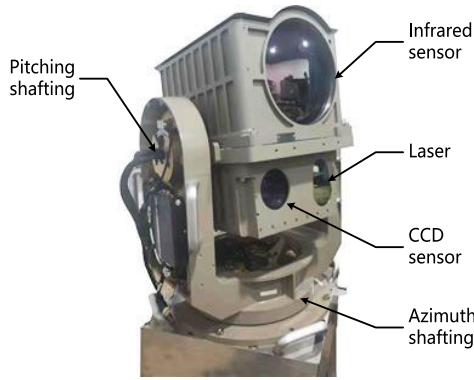
FIGURE 13. Experimental system.

TABLE 2. Step response error.

SPEED (°/S)	0.1	0.2	0.4	1.0	2.0
NO FTC	0.086	0.084	0.095	0.078	0.082
WITH FTC	0.016	0.015	0.018	0.014	0.015
PERCENTAGE OF REDUCTION	81.4%	82.1%	81.1%	82.1%	81.7%

fluctuate obviously. Moreover, the lower the starting speed of the system, the more serious the negative impact of this friction will be.

A low-speed start-up experiment was carried out using the system to verify the actual effect of friction torque compensation. With a low-speed step test signal to the system, we compared the speed output of the system under the conditions of non-friction torque compensation (Without FTC) with the friction torque compensation (with FTC), as shown in Figure 14.

The speed step response of the system was tested at 0.1°/s, 0.2°/s, and 1°/s, respectively. The dotted line and solid line in Fig.14 (a), (b), and (c) show the speed output response curves of the system without friction torque compensation and with friction torque compensation, respectively. From the experimental results, it can be seen that when the system has no friction torque compensation, the output of the system has an obviously delayed start-up, and after the start-up, the stability of the speed is very poor; and the lower the speed, the more intense the fluctuation of the speed. When starting at 0.1/s, there is an apparent slippage phenomenon, which accords with the action characteristics of the maximum static friction torque. When starting at 1°/s, and under the condition of friction torque compensation, the system can overcome the influence of friction and achieve the effect of a quick response. Table 2 shows the speed error test results when the system reached steady output in different speed tests.
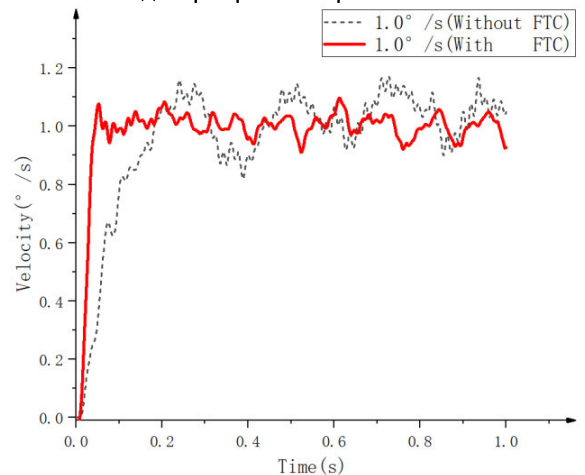
From the calculated results in the table, it can be seen that the low-speed control accuracy of the system with friction torque compensation is reduced by more than 80% compared to without friction torque compensation.
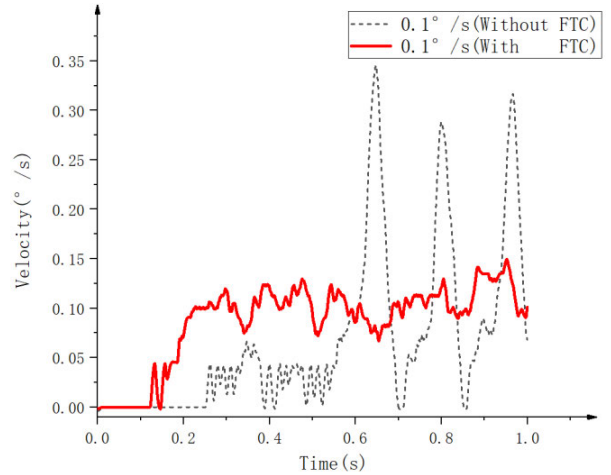
(a) Step response at a speed of 0.1 °/s.
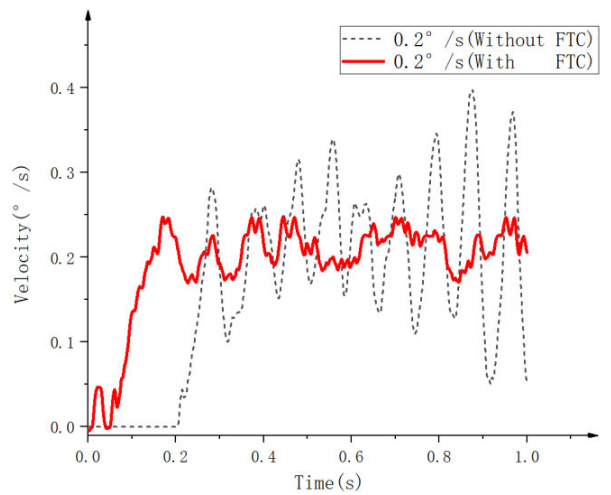
(b) Step response at a speed of 0.2 °/s.

(c) Step response at a speed of 1.0 °/s.

FIGURE 14. Step response analysis.

C. EXPERIMENT OF TRACKING LSS-UAV

The flying speed of the target is the key factor to determine the tracking accuracy of tracking equipment. The faster speed of
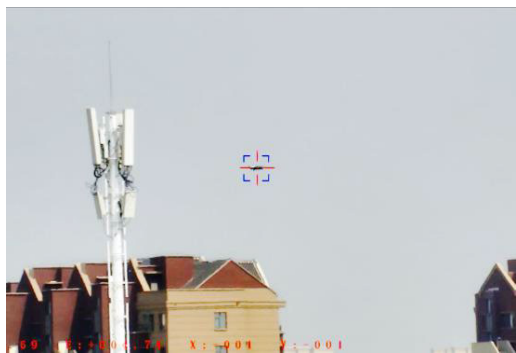
FIGURE 15. System tracking of the LSS-UAV.

the flying target, the lower precision of the tracking system will be obtained. Our team only focus on the influence of friction torque compensation and non-friction torque compensation on the tracking accuracy of the system under the same flight speed parameters. In the experiment, the UAV was tracked at a cruising speed of 20m/s(72km/h).

The frame frequency of the image sensor of the system is 50Hz, so the image processor needs to save one frame of data for data processing and output the processing result of the previous frame, so the output digital image information has a data delay of 20 millisecond(ms). According to the actual engineering test, the designed tracking closed-loop bandwidth is about 2Hz. The servo algorithm cycle of the controller is designed to be 1ms, and the design bandwidth of the speed closed loop is about 30Hz. The experimental scene is shown in Figure 15.

In the stable tracking stage of the system, because the deviation between the optical line of sight and the target needs to be constantly corrected, and the speed direction of the system needs to be constantly switched, it is inevitable that the low-speed friction force will be overcome in the process of changing the speed direction. In the experiment, the tracking accuracy is compared with that of the system speed loop with friction torque compensation and without friction torque compensation.

The tracking control system simultaneously locks and tracks the target. The tracking accuracy of the system was compared in conditions of with and without FTC.

The visible CCD sensor used in the system has a resolution of 1920 × 1080 pixel units, a lens focal length range of 15 ∼ 300mm, and the field angle corresponding to each pixel unit is 11.499μrad. Figure 16. shows the tracking accuracy of the system when the LSS-UAV flies at a speed of 20m/s.

Fig. 16(a) shows the tracking error of the system without friction torque compensation; From the data, the tracking accuracy (standard deviation) of the system is 1σ = 56.44 μrad; Fig. 16(b) shows the tracking error of the system after adding friction torque compensation. The tracking accuracy is 1σ = 14.86 μrad, which is reduced by more than three times compared to without friction compensation. This further verifies that the friction torque compensation of
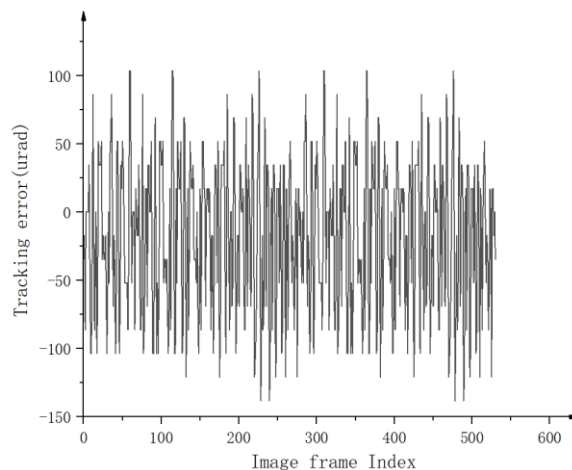
(a) Tracking accuracy without friction torque compensation
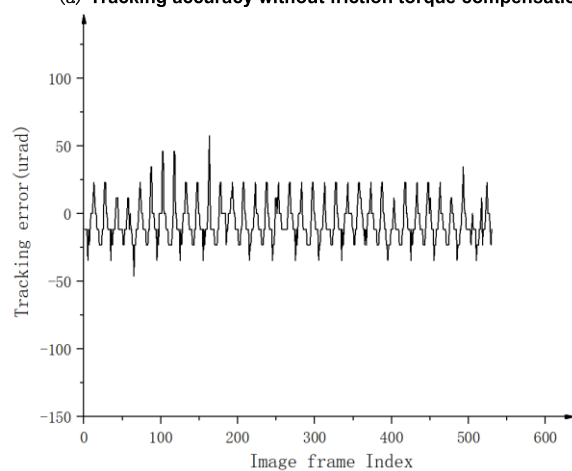
(b) Tracking accuracy with friction torque compensation

FIGURE 16. Tracking error.

the dynamic seal is beneficial to the speed control accuracy quality of the system, thus achieving the goal of smooth tracking of LSS-UAVs.

V. CONCLUSION

From the simulation and experimental results using our LSS_UAV tracker system, the control accuracy and speed stability of the closed-loop are improved with friction torque compensation, and the tracking accuracy for the LLS-UAV target is better. The friction torque model of the dynamic seal structure, composed of a labyrinth seal mechanism and magnetic fluid seal ring is accorded with the LuGre friction torque model.

In the early stage of modeling the friction torque model, we found that the proportion of friction torque brought by the magnetic fluid ring became weaker as the speed increased, and its influence could even be ignored at relatively high-speed. To simplify the complexity of the experiments, the influence of the eccentric installation of the magnetic fluid sealing ring and temperature change on friction torque were ignored. These influences are also an aspect that we will study further in the future.

If the motor is replaced by a brushless DC torque motor, the shafting friction could be further reduced. Combined with the current dynamic sealing measures, the speed control accuracy may also be further improved. We will also continuously improve the system design for the actual working effect of the system and the adaptability to specific environments.

REFERENCES

[1] Y. Wang, W. Li, Z. Huang, R. Tao, and P. Ma, "Low-slow-small target tracking using relocalization module," *IEEE Geosci. Remote Sens. Lett.*, vol. 19, pp. 1–5, 2022, doi: 10.1109/LGRS.2020.3043001.

[2] S. Musa, R. S. Abdullah, A. Sali, A. Ismail, and N. E. A. Rashid, "Low-slow-small (LSS) target detection based on micro Doppler analysis in forward scattering radar geometry," *Sensors*, vol. 19, no. 15, p. 3332, Jul. 2019, doi: 10.3390/s19153332.

[3] L. Jie, L. Chaofeng, D. Cheng, F. Tong, Z. Nimin, and Z. Hang, "Necessity analysis and scheme of constructing ultra-low-altitude defense system in megacities," *IEEE Aerosp. Electron. Syst. Mag.*, vol. 36, no. 1, pp. 14–21, Jan. 2021, doi: 10.1109/MAES.2020.3021303.

[4] W. Wei, J. Wang, Z. Fang, J. Chen, Y. Ren, and Y. Dong, "3U: Joint design of UAV-USV-UUV networks for cooperative target hunting," *IEEE Trans. Veh. Technol.*, early access, Nov. 9, 2022. [Online]. Available: https://ieeexplore.ieee.org/abstract/document/9944188

[5] L. Yang, H. Yao, J. Wang, C. Jiang, A. Benslimane, and Y. Liu, "Multi-UAV-enabled load-balance mobile-edge computing for IoT networks," *IEEE Internet Things J.*, vol. 7, no. 8, pp. 6898–6908, Aug. 2020, doi: 10.1109/JIOT.2020.2971645.

[6] J. Wang, C. Jiang, Z. Wei, C. Pan, H. Zhang, and Y. Ren, "Joint UAV hovering altitude and power control for space-air-ground IoT networks," *IEEE Internet Things J.*, vol. 6, no. 2, pp. 1741–1753, Apr. 2019, doi: 10.1109/JIOT.2018.2875493.

[7] C. Dong, C. Liu, J. Liu, N. Zhou, H. Zhang, and T. Fang, "An integrated scheme of a smart net capturer for MUAVs," *IEEE Access*, vol. 8, pp. 211820–211828, 2020, doi: 10.1109/ACCESS.2020.3037760.

[8] S. Yang, B. Tan, and X. Deng, "Numerical and experimental investigation of the sealing effect of a specific labyrinth seal structure," *Math. Problems Eng.*, vol. 2019, pp. 1–14, Jun. 2019, doi: 10.1155/2019/9851314.

[9] W. Zhou, Z. Zhao, Y. Wang, J. Shi, B. Gan, B. Li, and N. Qiu, "Research on leakage performance and dynamic characteristics of a novel labyrinth seal with staggered helical teeth structure," *Alexandria Eng. J.*, vol. 60, no. 3, pp. 3177–3187, Jun. 2021, doi: 10.1016/j.aej.2020.12.059.

[10] C. Han, H. Zhang, and J. Zhang, "Structural design and sealing performance analysis of biomimetic sealing ring," *Appl. Bionics Biomechanics*, vol. 2015, pp. 1–11, Jun. 2015, doi: 10.1155/2015/358417.

[11] L. Matuszewski, "New designs of centrifugal magnetic fluid seals for rotating shafts in marine technology," *Polish Maritime Res.*, vol. 26, no. 2, pp. 33–46, Jun. 2019, doi: 10.2478/pomr-2019-0023.

[12] J. Xu, Z. Li, H. Tang, W. Zheng, and X. Yuan, "Significant influence of nonlinear friction torque on motion performance of tracking turntables," *Tribology Int.*, vol. 136, pp. 148–154, Aug. 2019, doi: 10.1016/j.triboint.2019.03.059.

[13] C. Fan, Z. Chongfeng, and Y. Xiaolong, "Numerical analysis and experimental verification of magnetic fluid sealing for air cylinder in aerospace engineering," *Int. J. Appl. Electromagn. Mech.*, vol. 66, no. 4, pp. 581–597, Aug. 2021, doi: 10.3233/JAE-201572.

[14] Y. Mitamura, S. Takahashi, S. Amari, E. Okamoto, S. Murabayashi, and I. Nishimura, "A magnetic fluid seal for rotary blood pumps: Effects of seal structure on long-term performance in liquid," *J. Artif. Organs*, vol. 14, no. 1, pp. 23–30, Mar. 2011, doi: 10.1007/s10047-010-0526-8.

[15] S. Huang, W. Liang, and K. K. Tan, "Intelligent friction compensation: A review," *IEEE/ASME Trans. Mechatronics*, vol. 24, no. 4, pp. 1763–1774, Aug. 2019, doi: 10.1109/TMECH.2019.2916665.

[16] S.-H. Cho, Y.-S. Kim, and J.-Y. Kim, "Friction compensation of electric-motor driven revolute joint with harmonic gear," *J. Korean Soc. Manuf. Technol. Engineers*, vol. 29, no. 3, pp. 259–265, Jun. 2020.

[17] M. Kim, F. Beck, C. Ott, and A. Albu-Schäffer, "Model-free friction observers for flexible joint robots with torque measurements," *IEEE Trans. Robot.*, vol. 35, no. 6, pp. 1508–1515, Jul. 2019, doi: 10.1109/TRO.2019.2926496.

[18] P. Cui, D. Zhang, S. Yang, and H. Li, "Friction compensation based on time-delay control and internal model control for a gimbal system in magnetically suspended CMG," *IEEE Trans. Ind. Electron.*, vol. 64, no. 5, pp. 3798–3807, May 2017, doi: 10.1109/TIE.2016.2644620.

[19] H. Yang, Y. Zhao, M. Li, and Y.-J. Zhou, "Study on the friction torque test and identification algorithm for gimbal axis of an inertial stabilized platform," *J. Aerosp. Eng.*, vol. 230, no. 10, pp. 1990–1999, Aug. 2016, doi: 10.1177/0954410015620709.

[20] X. Wang and S. Wang, "Output torque tracking control of direct-drive rotary torque motor with dynamic friction compensation," *J. Franklin Inst.*, vol. 352, no. 11, pp. 5361–5379, Nov. 2015, doi: 10.1016/j.jfranklin.2015.08.021.

[21] J. Hu, Y. Wang, L. Liu, and Z. Xie, "High-accuracy robust adaptive motion control of a torque-controlled motor servo system with friction compensation based on neural network," *Proc. Inst. Mech. Engineers, C, J. Mech. Eng. Sci.*, vol. 233, no. 7, pp. 2318–2328, Apr. 2019, doi: 10.1177/0954406218783017.

[22] M. Zhang, M. Zhou, H. Liu, B. Zhang, Y. Zhang, and H. Chu, "Friction compensation and observer-based adaptive sliding mode control of electromechanical actuator," *Adv. Mech. Eng.*, vol. 10, no. 12, pp. 1–15, Dec. 2018, doi: 10.1177/1687814018813793.

[23] B. Li, Y. Zhang, L. Yuan, and X. Xi, "Study on the low velocity stability of a prostate seed implantation Robot's rotatory joint," *Electronics*, vol. 9, no. 2, p. 284, Feb. 2020, doi: 10.3390/electronics9020284.

[24] Z. Xinli and X. Li, "A finite-time robust adaptive sliding mode control for electro-optical targeting system with friction compensation," *IEEE Access*, vol. 7, pp. 166318–166328, 2019, doi: 10.1109/ACCESS.2019.2953997.

[25] X. Wang, S. Lin, and S. Wang, "Dynamic friction parameter identification method with LuGre model for direct-drive rotary torque motor," *Math. Problems Eng.*, vol. 2016, pp. 1–8, 2016, doi: 10.1155/2016/6929457.

[26] Y. Su, Q. Wang, F. Yan, and Y. Huang, "Friction compensation for an M-level telescope based on high-precision LuGre parameters identification," *Res. Astron. Astrophys.*, vol. 21, no. 1, p. 019, Feb. 2021. [Online]. Available: https://iopscience.iop.org/article/10.1088/1674-4527/21/1/19/meta

ZHUQIU GAIT was born in 1973. From 1998 to 2018, he worked at the Aviation Imaging and Measurement Department, Changchun Institute of Optics, Fine Mechanics and Physics, Chinese Academy of Sciences. Since 2018, he has been teaching with the Institute of Optoelectronic Engineering, Changchun University of Science and Technology mainly engaged in research and teaching of the servo control system and angle measurement system of aviation gyro stabilized platform and vehicle stabilized platform. He is a member of the China Society of Optical Engineering.

JINSONG WANG was born in 1973. He is currently a Professor and a Ph.D. Supervisor and works with the Institute of Optoelectronic Engineering, Changchun University of Science and Technology mainly engaged in research of photoelectric testing technology and instruments, photoelectric precision measurement, and digital twin technology. His research interests include photoelectric testing technology and instruments, mainly focuses on the detection of performance parameters of white light, infrared, and laser sight. He is a member of the Image Science and Engineering Branch of China Instrumentation Society.

● ● ●